Vacuolization in Cytoplasm and Cell Membrane Permeability Enhancement Triggered by Micrometer-Sized Graphene Oxide

Congyu Wu,[†,§] Chong Wang,[‡,§] Jing Zheng,[‡] Chao Luo,[‡] Yanfang Li,[‡] Shouwu Guo,[*,†] and Jingyan Zhang[*,‡]

[†]Department of Electronic Engineering, School of Electronic Information and Electrical Engineering, Shanghai Jiao Tong University, Shanghai 200240, P.R. China and [‡]State Key Laboratory of Bioreactor Engineering, Shanghai Key Laboratory of New Drug Design, School of Pharmacy, East China University of Science and Technology, Shanghai, 200237. P.R. China. [§]C. Wu and C. Wang contributed equally to this work.

ABSTRACT A deep understanding of the interaction of a graphene oxide (GO) sheet with cells at the molecular level may expedite its biomedical application and predict its new functions and adverse effects. Herein we inspect the interaction between micrometer-sized GO (mGO), commonly used in biomedical research, and cells at the molecular level through a variety of techniques. A major finding is that, instead of direct cellular penetration, the mGO sheets can stimulate the cellular response by interacting with the membrane protein and the membrane. Specifically, it is illustrated that even within a short exposure time the mGO sheets can induce the formation of vacuoles in the cytosolic compartment and enhance the cell permeability. The vacuolization is only observed in the cells that strongly express aquaporin (AQP1), indicating the specific interaction of the mGO with AQP1. Moreover, inhibition of the AQP1 activity prevents the formation of vacuoles, revealing that the interaction of the mGO with AQP1 occurs most probably at the vestibule of AQP1 at the extracellular side. Additionally, though the cell permeability was enhanced, it only improves the penetration of small molecules, not for macromolecules such as proteins. These findings are potentially valuable in cancer therapy because AQPs are strongly expressed in tumor cells of different origins, particularly aggressive tumors, and it will also be beneficial for drug transport across barrier membranes.

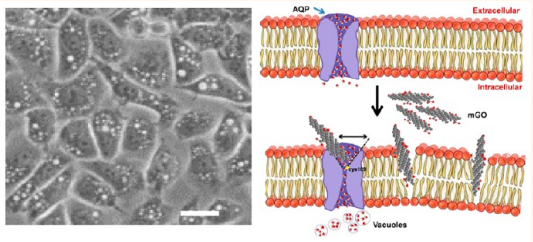

KEYWORDS: micrometer-sized graphene oxide · mGO · aquaporins · AQPs · cell membrane

The emerging applications of graphene oxide (GO) in anticancer drug delivery,[1−3] gene transfection and delivery,[4,5] cell and tumor imaging,[6−8] protein inhibition,[9] photothermal therapy,[10,11] and DNA manipulation[12,13] have aroused the need to deeply understand the interaction of GO with cells at the molecular level to expedite practical applications, envisaging new functions and adverse effects. It was generally believed that GO with nanometer lateral sizes (nGO) might be engulfed by cells through endocytosis, resulting in disruption of the cytoskeleton as graphitic nanoribbons,[14] programmed necrosis on macrophages, and massive reactive oxygen species (ROS) generation, which reduce cell viability and undermine macrophagic morphology and functions.[15] On the other hand, the micrometer-sized GO (mGO) sheets could be taken by cells through the phagocytotic pathway,[16] but it took a longer time for them to penetrate the cells compared to nGO.[17] It was demonstrated that the mGO can induce *in vitro* and *in vivo* mutagenesis only after 24 h or even longer incubation, suggesting the difficulty of the mGO sheets in cellular penetration.[18] Alternatively, it was also speculated that GO sheets might not be engulfed by cells; instead, they could be absorbed on the cell membrane as the first step.[16] Thus, the GO may affect the cellular processes *via* the interaction with the cellular membrane or membrane proteins.[19] Additionally, the theoretical study showed that the bending stiffness of mGO sheets was close to that of lipid bilayers of cells, supporting the possibility of the interaction between GO and membrane proteins.[20] Very recent work

* Address correspondence to swguo@sjtu.edu.cn, jyzhang@ecust.edu.cn.

Received for review November 21, 2014 and accepted July 16, 2015.

Published online July 24, 2015
10.1021/acsnano.5b01685

demonstrated that the interaction between GO and Toll-like receptor 4 (TLR4), a single membrane-spanning receptor, could induce TNF-α production that usually triggers the programmed necrosis on macrophages in an autocrine loop, and notably, the macrophage uptake of GO may not be required for induction of necrosis.[15] Based on coarse-grained and all-atom molecular dynamics, analytical modeling, confocal laser scanning microscopy (CLSM) fluorescence imaging, and electron microscopic imaging, Li *et al.* proposed that multilayered GO sheets could directly penetrate the lipid bilayer and enter cells at edge asperities and corner sites.[21] More interestingly, it was believed that the strong dispersion interaction between GO sheets and lipid molecules could result in the extraction of a large amount of phospholipids from *Escherichia coli* membranes during the penetration.[22] Chances that mGO interacts with the cell membrane in these modes, however, might be slim compared to other weak interactions, such as hydrogen bonding, electrostatic, and hydrophobic interactions. Nevertheless, these findings suggest the possibility that the mGO sheets elicit their cellular level effect *via* interaction with membrane or membrane proteins without penetrating the cells. Actually, it was shown recently that GO sheets could disturb the cell membrane of bacterial and fungal spores and might induce the decrease of the bacterial membrane potential and the leakage of electrolytes of fungal spores.[23] However, information on the interaction of GO sheets, especially mGO, that are often used in biomedical research, with cells at the molecular level, remains to be elaborated.

Here, we describe the interaction of mGO with cells at the molecular level. We demonstrate that mGO sheets do not enter the cells within a short exposure time; instead, they interact with the membrane protein, aquaporins (AQPs), of the cells and induce the formation of vacuoles in the cytosolic compartment. In addition, due to the interaction of mGO with the cell membrane, the permeability of the cells is also enhanced. The findings might open a novel biomedical application of mGO because AQPs are strongly expressed in tumor cells of different origin.[24]

RESULTS

mGO Induces the Formation of Vacuoles in the Cytoplasm. The mGO used in this work was obtained following the procedure described in our previous work.[25] They adopt a single atomic layer structure with a thickness of about 1 nm and a lateral size of 0.5−4 μm, in which about 71% range between 0.8 and 2 μm, and were characterized with atomic force microscopy and UV−vis, IR, and Raman spectroscopies (Supporting Information Figure S1).[25,26] As mentioned previously, these mGO sheets could penetrate into the cells after 24 h or even longer incubation times. However, within a short incubation time, the mGO cannot (or is difficult to) be taken by the cells.[16,17,27] To understand this phenomenon, the mGO sheets were incubated with MCF-7 cells from 20 min to 24 h. Unexpectedly, small light-colored vacuoles were spotted inside the cell under an optical microscope in a short incubation time (Figure 1). The size and number of vacuoles were amplified with increasing incubation time and concentration of mGO in the culture (Figure 1 and Supporting Information Figure S2). These phase-lucent vacuoles were absent in the control group without mGO (Supporting Information Figure S2, row c). No sign of loss of membrane integrity, cell lysis, shrinking of cytoplasm, condensation of nucleus, or fragmentation of cells into smaller bodies was observed. Similarly, vacuoles were also found in the stomach cancer MGC-803 cells, human gastric cancer SGC-7901 cells, human gastric adenocarcinoma cell line AGS, lung cancer A549 cells, HeLa cells, and GES-1 cells under the same experimental conditions (Figure S3). Such vacuoles are quite similar to the lysosomes upon chemical treatment or stress conditions.[28] To further identify these vacuoles, the MCF-7 cells incubated with mGO were examined by transmission electron microscopy (TEM) after being fixed. As shown in Figure 1g,h, a number of vacuoles with variable sizes were observed in the cytoplasm of MCF-7 cells, similar to the aforementioned optical microscope imaging results. More clearly, the high-magnification TEM image (Figure 1h) shows that most of the intracellular vacuoles have irregular shapes and lack a distinguishable double-layered membrane, suggesting that they might not be lysosomes or autophagosomes.[29] The low electron density inside the vacuoles also indicates that they are not mGO,[17,21] and there are no other organelles or their fragments within these vacuoles.

As-Induced Vacuoles Are Neither Lysosomes nor Autophagosomes. To further confirm whether the as-induced vacuoles contain any organelles, their fragments, or proteins, MCF-7 cells were first transfected transiently with the PSICOR-GFP plasmid and then incubated with mGO. As depicted in Figure 2c, there is apparently no green fluorescence inside the vacuoles (black dots in Figure 2c), revealing that there is no protein in them. By comparing Figure 2b,d, it can be found that vacuoles are not stained by lysotracker red either, implying that the vacuoles are not acidic. These data clearly verify that the vacuoles are neither lysosomes nor mGO sheets taken by the cells.

Vacuolization in the cytoplasm is a typical morphological feature of cellular autophagy,[30] thereby it is possible that the vacuoles observed might be autophagosomes. Figure 2e displays the images of the MCF-7 cells incubated with 100 μg mL^{-1} of mGO in the presence of 10 mM 3-methyladenine (3-MA), a widely used inhibitor of autophagy.[31] The inhibitor 3-MA apparently did not block the vacuolization

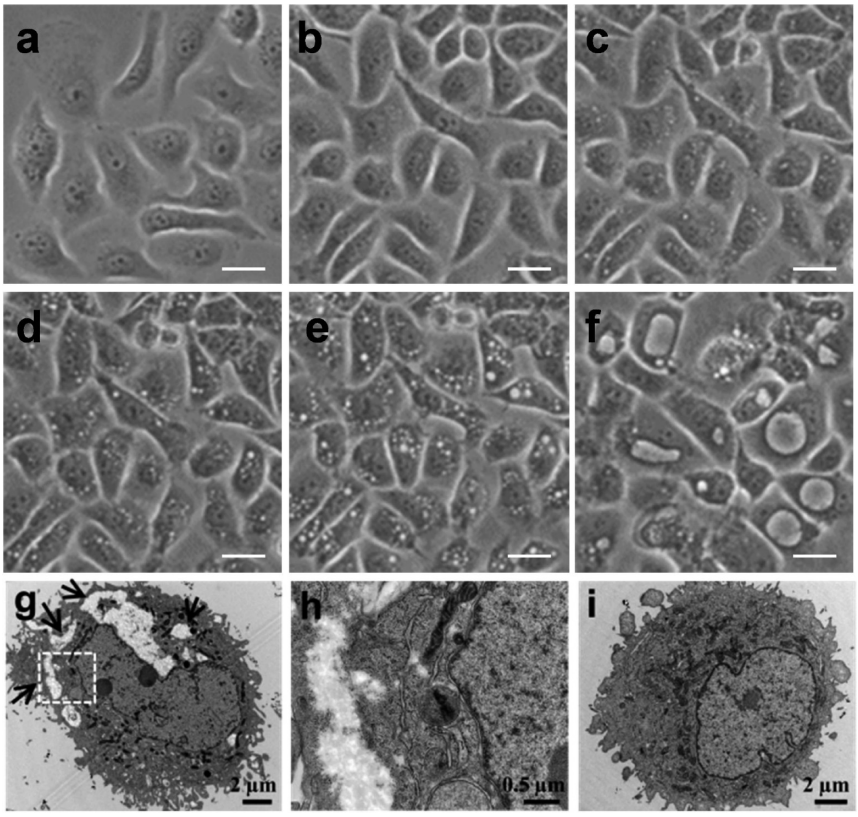

Figure 1. mGO induces the formation of vacuoles. Microscopy images of the MCF-7 cells incubated with 50 μg mL^{-1} of the mGO for (b) 20 min, (c) 1.5 h, (d) 3 h, (e) 6 h, and (f) 24 h. Control cells in the absence of mGO (a). Scale bar: 20 μm. TEM images of the MCF-7 cells incubated with mGO (200 μg mL^{-1}) for 1.5 h; arrows indicate the vacuoles (g). High magnification of the vacuoles (h). TEM image of the control MCF-7 cell (i). Each experiment was repeated at least three times.

induced by mGO, indicating that the vacuoles are not autophagosomal in origin, which is in agreement with the absence of the double-layer membrane shown by TEM (Figure 1g,h). To further corroborate the result, MCF-7 cells were transfected with the GFP-LC3 plasmid. LC3 is microtubule-associated protein light chain 3 that targets the phosphatidyl ethanolamine on autophagosome membranes, thus the relative amount of bright LC3 puncta that are flagged by the fluorescence of GFP correlates with the number of autophagosomes in the cell.[29,32] As shown in Supporting Information Figure S4a, intracellular vacuoles did not overlap with the smaller green fluorescent autophagosomes. In fact, autophagosomes often fused with lysosomes, forming autophagolysosomes that can be tracked by lysosome tracker.[29] However, the overlap of green and red fluorescence of the lysosome tracker and vacuoles did not occur either (Supporting Information Figure S4c). These results together show that the vacuoles induced by mGO sheets are neither lysosomes nor autophgosomes.

Formation of Vacuoles Slows Cell Proliferation. It was generally accepted that mGO exhibited cytotoxicity because it may stimulate a series of cellular responses after being taken by the cells.[15−18,33,34] However, with a short incubation time (1.5 h), cells could not take mGO quickly[17,35] and the formation of vacuoles is therefore probably a result of cellular responses upon exposure to mGO. These responses could be related to activities such as diffusion, osmosis, mediated transport, *etc*. that occurred on the cell membrane, which may be analogous to the generation of autophagosomes within cells upon starvation.[36] Even though numerous vacuoles were spotted inside the cells, there was no phenotypic sign of necrosis or apoptosis, and the cells were in a healthy state (Figure 1). The vacuoles were also observed under microscope in two daughter cells, suggesting that vacuoles are probably inherited in cell proliferation (Figure S5). Nevertheless, the cell proliferation assay was performed with the cells incubated with different amount of mGO for 3 h, and no obvious cytotoxicity was observed (Figure 3a). The cytotoxicity of the mGO was low, and 86% of cells were still alive even after 24 h of incubation with 100 μg mL^{-1} of the mGO (Supporting Information Figure S6). However, we found that the proliferation rate of the cells indeed slowed when the cells were washed with phosphate-buffered saline (PBS) twice after incubation with mGO and reincubated in a complete culture medium for another 1, 2, and 3 days. With the increased concentration of mGO, the effect was more pronounced (Figure 3a). Meanwhile, it was also found that, with the increase of incubation time, the cell recovery rate was slow but could eventually get back to their regular state. The results provide a hint that

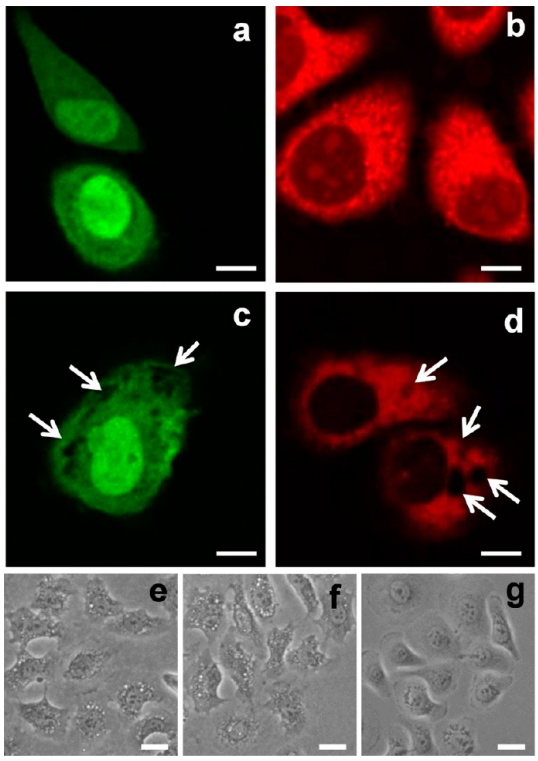

Figure 2. Vacuoles are not lyzosomes or autophagosomes. (a) CLSM fluorescence image of the PSICOR-GFPDNA transfected MCF-7 cells. (b) Fluorescence image of the MCF-7 cells that were stained with lysotracker. (c) Transfected MCF-7 cells incubated with mGO (20 μg mL^{-1}) for 3 h. (d) Fluorescence images of the MCF-7 cells that were pretreated with mGO (20 μg mL^{-1}) and then stained with lysotracker. Scale bar: 10 μm. (e,f) Microscopy images of MCF-7 cells that were treated with mGO (100 μg mL^{-1}) in the presence and absence of 10 mM 3-methyladenine for 1.5 h. (g) Images of the cells that were incubated with 10 mM 3-methyladenine alone as a control.

something might occur inside the cells when they were incubated with mGO. Optical microscope images of the cells revealed that the vacuoles in the mGO-treated cells fused to each other, forming larger vacuoles during the cell incubation in the fresh medium on the first day (Supporting Information Figure S7b). The large vacuoles then disappeared gradually during the following 2 days of incubation (Supporting Information Figure S7c,d), and the cells returned to their normal status.

The heterogeneity of the vacuoles for different incubation times was quantified by counting the number and size of the vacuoles per 20 cells. As shown in Figure 3b, after the incubation with mGO for 3 h, most generated vacuoles are smaller in size, less than 2 μm, while with the time increase, the size of the vacuoles grows and some are 5−12 μm; a few even grow to 20−30 μm when the cells are incubated for 1−2 days. Interestingly, the number and size of the vacuoles decrease on the third day of incubation, and only a few small-sized vacuoles exist. This process was also monitored by flow cytometric measurement to examine the effect of vacuoles on the cell cycles, which are more informative to the cell growth process.[37] As shown in Figure 3c−e, compared to the control cells, cell cycles were dramatically affected after the incubation with mGO for 3 h (Figure 3d); about 37.5% of the cells were arrested in S phase, while in the control cells, it was only 19%. To display the difference clearly, panels c and d in Figure 3 were overlapped and are displayed in Figure S8. The recovery of the mGO-treated cells after the reincubation in fresh culture medium is accompanied by the decrease of S phase population. To further quantify the number and size of the vacuoles spotted at different phases of a cell cycle, fluorescence ubiquitination cell cycle indicator (FUCCI), a fluorescent protein (FP)-based sensor that employs a red (RFP) and a green (GFP) fluorescent protein fused to different regulators of the cell cycle, was employed.[38] The dynamic color change from red to yellow to green indicates the progression of the cell from G1, G1/S transition and S, G2, M phases. As shown in Figure 3f, there are more vacuoles at the G1/S phase than at the other phases, and the vacuoles with 1−2 μm size only appeared in the G1/S phase, too. Combining these results together with the flow cytometric data, one can see that the cells are arrested at S phase, where the maximum number and the largest vacuoles are found, suggesting that possibly a certain number and size of vacuoles could affect the cell phases, eventually affecting cell proliferation. This result is different from the effect of longer incubation with mGO to the cells, in which mGO sheets were engulfed by the cells.[17,18] Vacuolization was not observed in the cells incubated with nanometer-sized GO even for longer incubation time, possibly due to their small size (Supporting Information Figure S9). S phase arrest induced by mGO suggests the DNA damage may occur at a certain point, leading to a slow proliferation.[39] The recovery from S phase arrest, on the other hand, indicated the restoration of DNA synthesis after mGO sheets were removed. Even though the vacuoles were formed in the cytoplasm, the cellular activity was still affected, further highlighting that the formation of vacuoles is a stimulus response of the cells to the mGO rather than a consequence of the cellular uptake. More importantly, the results also specify that vacuoles possibly contain water or liquid of small molecules that are not harmful to the cells because the enlargement, collapse, and the disappearance of the vacuoles occurred at the stage of the cell recovery instead of cell death (Supporting Information Figure S7).

Origin of the Vacuoles. The fact that vacuoles affect the cell proliferation and the affected cells could recover after the removal of mGO, that there are no proteins in the vacuoles, and the vacuoles have low density under optical microscopy and low electron density under TEM, prompted us to examine the origin of vacuoles. To do this, the vacuolated MCF-7 cells were first incubated in a hypertonic PBS solution, and some

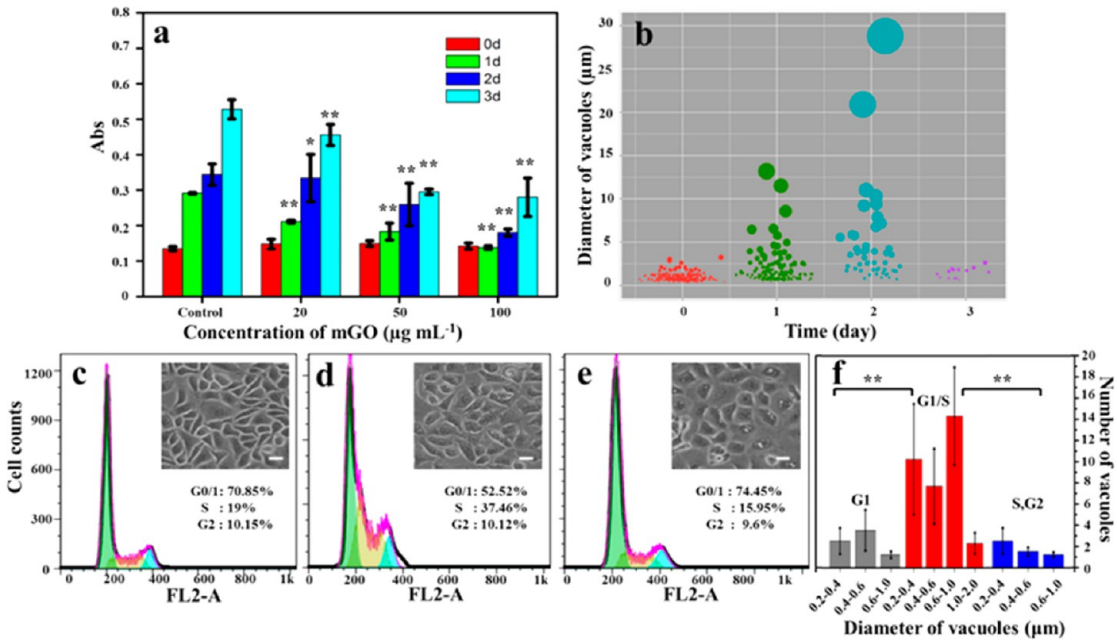

Figure 3. Effect of the vacuoles induced by mGO on the proliferation and cycle of MCF-7 cells. (a) Cells were first incubated with mGO (20, 50, and 100 μg mL^{-1}) for 3 h (0 day) and then washed with PBS twice and reincubated in a complete culture medium for another 1, 2, and 3 days. Cells grown in a complete culture medium without mGO were the control. Data represent mean $\pm$ SD; the experiment was performed three times; *t* test, *$p < 0.05$ and **$p < 0.01$. (b) Number and size of the vacuoles found in the cells after different incubation time. The sizes of circles indicate their relative sizes. The number of the cells that counted were 20 at each incubation time. (c–e) Flow cytometric analysis of the cell cycles of the MCF-7 cells that were incubated with RPMI 1640 medium (c) and mGO (100 μg mL^{-1}) for 3 h (d) and were recultured in fresh culture medium for another 3 days (e). Insets are bright-field microscopy images of the corresponding cells (scale bars: 20 μm). (f) Number and size of the vacuoles found in different phases of cell cycle, which were determined using a cell cycle indicator. Data represent mean $\pm$ SD; *t* test, **$p < 0.01$.

vacuoles diminished 1 h later, as indicated by arrows in Figure 4b. In the control group (Figure 4c), the number of vacuoles remains roughly the same. The disappearance of the vacuoles in the cytoplasm in hypertonic solution is a positive sign that they are likely associated with water transport of the cells, and in other words, vacuoles may contain water. The assumption was further supported by the morphological transform of the suspended cells when exposed to the culture medium containing a high concentration of mGO. Figure 4e,f shows the images of the suspended MCF-7 cells that were incubated with the mGO for 1.5 and 3 h, respectively. With the incubation time increase, some cells started to develop protrusions (indicated by arrows). Such phenomenon was not noted in the control cells that were incubated with regular PBS. The result showed evidently that the incubation with mGO enhanced the water influx of the cells.

Generally, water influx in mammalian cells is either through the membrane by diffusion, macropinocytosis, and/or through water channels, more specifically, aquaporins.[40,41] Free diffusion is a slow and inefficient process that may not be a major water transport process in our case. Macropinocytosis is a nonselective internalization process of fluid,[41,42] which is relatively efficient and thus is possible in this case. However, extracellular fluid tracer, lucifer yellow (LY), in the medium was taken up in the mGO-treated cells in 15 min, but LY was not found in the vaculoles, as shown in Figure 5, precluding that the vacuoles are formed through macropinocytosis. It should be noted that LY can be taken by mGO-treated cells but not the control cells, implying that the permeability of the cells is probably changed (see Discussion).

AQP is a highly efficient water transport channel. AQP1, a typical AQP, is strongly expressed in the membrane of breast cancer cell line MCF-7;[43,44] we first examined whether the vacuole formation induced by mGO is linked to AQP1 by inhibiting its transport activity. Actually, the transport ability of the AQP1 can be blocked specifically by Hg^{2+}, for which it reacts with the sulfhydryl of cys189 that is located close to the entrance of the water channel.[45] When MCF-7 cells were first incubated with $HgCl_2$ and then exposed to the mGO, we found, unexpectedly, that there was almost no vacuole formed in the cell plasma (Figure 6a). It was also found that the cells were first treated with $HgCl_2$ followed by incubation with β-mercaptoethanol, which easily binds to $HgCl_2$, and finally with mGO, vacuoles appeared again (Supporting Information Figure S10a). In contrast, vacuoles were not observed in the control cells that were pretreated with $HgCl_2$ and β-mercaptoethanol without further incubation with mGO (Supporting Information Figure S10b,c). The inhibition of AQP1 transport activity by $HgCl_2$ apparently also hinders the formation of vacuoles

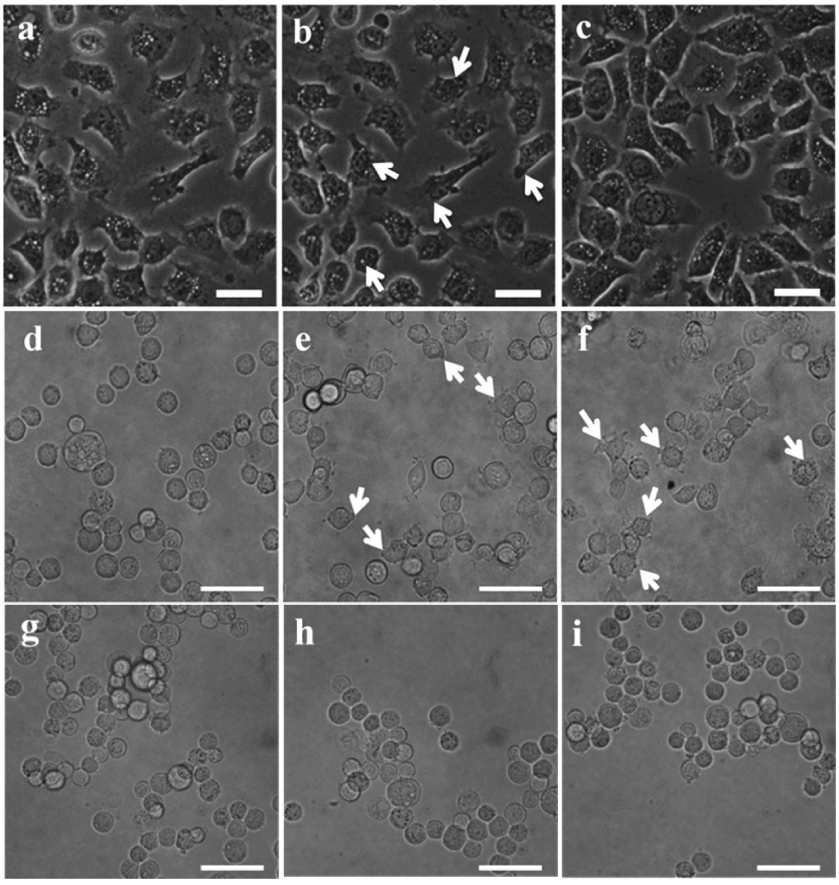

Figure 4. Vacuoles are associated with water influx of cells. Microscopy images of the adherent MCF-7 cells that were incubated with 100 μg mL^{-1} of mGO for 1 h (a). The preincubated cells were reincubated in hypertonic PBS solution (145 mM NaCl) (b). Reincubated cells were then cultured in regular PBS solution (scale bar: 20 μm) (c). Microscopy images of the suspended MCF-7 cells incubated with 200 μg mL^{-1} of mGO for 0, 1.5, and 3 h (d−f) (scale bar: 50 μm). (g−i) Controls of the suspended MCF-7 cells incubated without mGO for 0, 1.5, and 3 h, respectively.

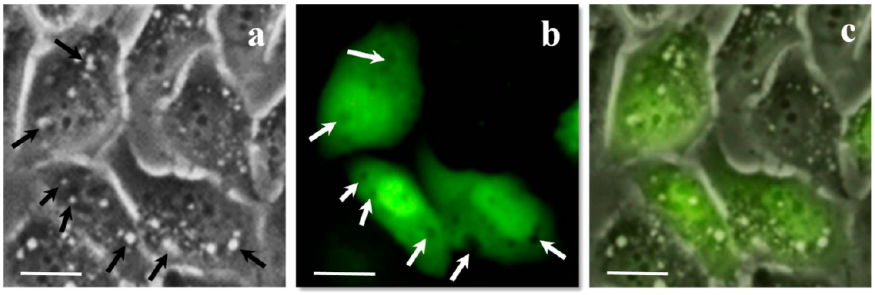

Figure 5. Vacuoles were not formed *via* macropinocytosis. Microscopy images of the mGO-treated MCF-7 cells that were incubated with lucifer yellow (0.5 mg mL^{-1}) in PBS for 15 min. (a) Bright-field image of the cells; (b) fluorescence image of the cells excited at 450 nm; (c) overlay of (a) and (b). Scale bar: 15 μm. Arrows indicate the vacuoles.

induced by mGO. The inhibitory experiments were also carried out with another two inhibitors, acetazolamide and $HAuCl_4$, and similar results were obtained (Supporting Information Figure S11).[46,47] These results provide solid evidence that the formation of vacuoles is associated with AQP1 of the cells. Further, these findings also reveal that the mGO does not interfere with the narrow water channel of AQP1.[48]

To reach a more definitive conclusion, similar experiments were performed on AQPs that are abundant in human erythrocytes.[49] As displayed in Supporting Information Figure S12, the hemolysis of human erythrocytes is proportional to the concentration of mGO in the culture medium, and $HgCl_2$ also could inhibit the hemolysis that was induced by the mGO, which is very consistent with the observation on MCF-7 cells. Under optical microscopy, the burst of the human erythrocytes was observed as early as 20 min of the incubation with a lower ratio of mGO to cell numbers (compared to the experimental conditions used with MCF-7 cells),

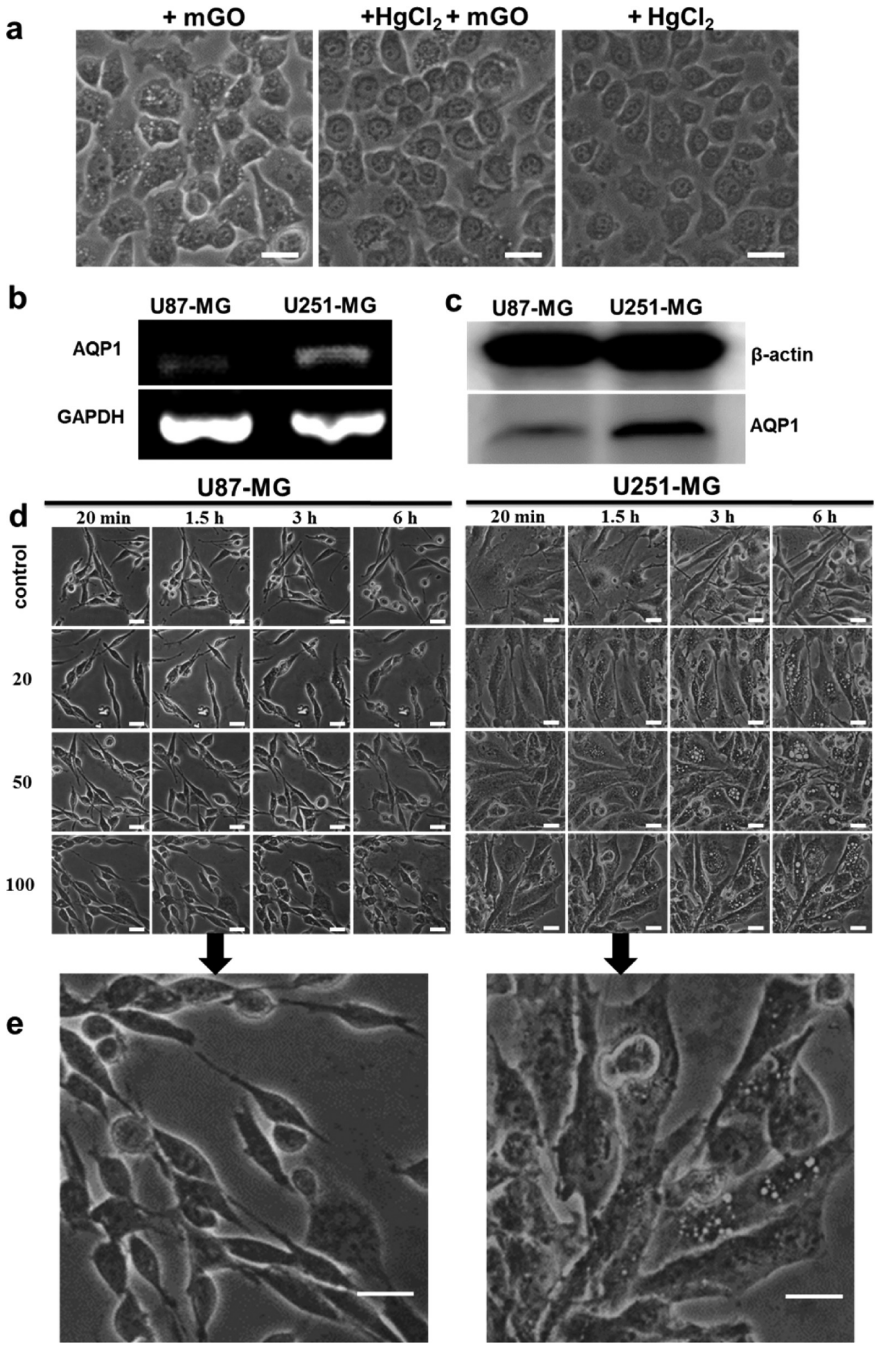

Figure 6. Vacuole formation is associated with the AQP1 of the cells. (a) Microscopy images of the MCF-7 cells that were treated with mGO (100 μg mL^{-1}) for 1.5 h without and with $HgCl_2$ pretreatment (200 μM). Control cells were pretreated with 200 μM of $HgCl_2$ only. Scale bar: 20 μm. (b) mRNA expression of AQP1 in U87-MG and U251-MG cells. RT-PCR was used to amplify AQP1 present in the two cell lines. (c) Western blot analysis of AQP1 protein expression in U87-MG and U251-MG cells. (d) Comparison of the microscopy images of the U87-MG and U251-MG cells incubated with 20, 50, and 100 μg mL^{-1} of the mGO for 20 min, 1.5 h, 3 h, and 6 h. Scale bar: 20 μm. (e) Blown-up images of the U87-MG and U251-MG cells incubated with 100 μg mL^{-1} of mGO for 1.5 h. Scale bar: 20 μm.

which is possibly because erythrocytes are rich in AQPs. When the mGO-treated human erythrocyte suspension solution was transferred into a confocal dish, vacuoles were observed (Figure S13), which indicated that mGO-evoked hemolysis of erythrocytes is related to their vacuolization induced by the mGO. In fact, mGO-induced hemolysis of human erythrocytes was reported previously, but it was believed that hemolysis was caused by ROS that generated upon GO exposure for 24 h.[50]

Encouraged by the aforementioned results, we carried out a further study with two human glioma cell lines, U87-MG and U251-MG, because the expression of AQP1 is much stronger in the latter than in the former at protein and RNA levels, as shown in Figure 6b,c, and reported in the literature.[51] Additionally, glioma cells

quickly adjust their cell volume in response to osmotic challenges as they invade into the narrow and tortuous extracellular spaces of the brain primarily through AQPs.[51] Figure 6d compares the effect of mGO on these two cell lines under the same conditions. Similar to MCF-7 cells, intracellular vacuoles were observed in U251-MG cells with the concentration of mGO as low as 20 μg mL^{-1} after 1.5 h of incubation. No vacuole was spotted in U87-MG cells even with a high concentration of mGO for a longer incubation time. Figure 6e show the blown-up images of these two cell lines under the same conditions. We also checked the AQP1 expression level in MCF-7, A549, AGS, and SGC7901 cells, and all of them have a high AQP1 expression level (Figure S14). These findings unambiguously convinced us that mGO sheets interact with the cells *via* membrane protein AQP1, eventually resulting in the formation of vacuoles.

DISCUSSION

We have inspected the interaction of the mGO with the cells within a short exposure time. Generally, the cytotoxicity of mGO was believed to be *via* cellular uptake, but in fact, it is difficult for the mGO used in this research to penetrate cells very rapidly. Hence, mGO probably influences the cells *via* interaction with the cell membrane and/or membrane protein. AQPs are membrane proteins that are heavily expressed in many human cell lines. They are tetramers, and each monomer serves as a water channel. The monomer has six transmembrane α-helices arranged in a right-handed bundle, with five interhelical loop regions that form the extracellular and cytoplasmic vestibules.[48] Two hydrophobic loops contain an asparagine-proline-alanine motif, which overlaps the middle of the lipid bilayer of the membrane forming a 3-D "hourglass" structure where water flows through.[48] The hourglass geometry of AQP1 reduces the end effects and maximizes water permeability.[52] We may simplify the hourglass structure of APQ1 by assuming that it is made of a central cylinder water channel connected with two conical vestibules (Figure 7). $HgCl_2$, an AQP1 inhibitor, can block the formation of vacuoles induced by the mGO, indicating that the mGO did not interfere with the central cylinder region of AQP1. The only site that mGO possibly interacts with should be the vestibule of AQP1 at the extracellular side, at which it may modulate the angle of the conical entrance of AQP1 by expanding its opening (indicated by the arrow in Figure 7). It was shown that the conical entrance of the hourglass structure of AQP1 with a suitable opening angle can indeed provide a large increase of the hydrodynamic channel permeability.[52] The hydrophobic interaction between mGO and AQP1 is expected because mGO has a large hydrophobic basal plane,[53] which had been shown that it could interact with the proteins;[54] several conserved hydrophobic residues lining the aqueous

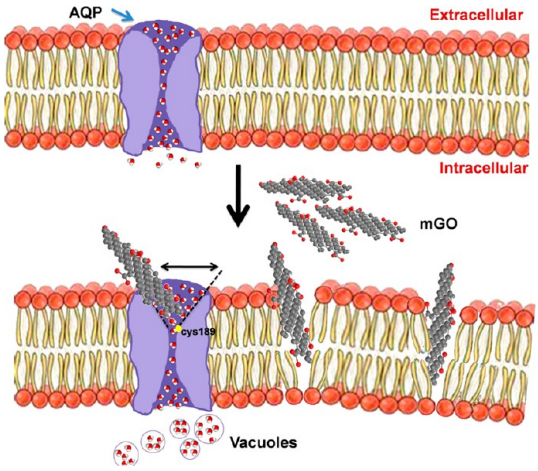

Figure 7. Schematic drawing of the interaction of mGO with AQPs and the membrane.

pathway of AQP1 permit rapid and efficient water transport;[48,54] they thus could interact with mGO. To verify the hydrophobic interaction between AQP1 and mGO, optical microscopy images of the MCF-7 cells after the incubation with identical concentration of the mGO and chemically reduced mGO (CR-mGO1 (moderately reduced) and CR-mGO2 (deeply reduced)) were compared (Supporting Information Figure S15). The deeper the reduced mGO is, the more hydrophobic it is.[54] Apparently, the more hydrophobic mGO is, the more vacuoles were generated, suggesting the stronger hydrophobic interaction between mGO and AQP1. The result was also supported by the finding that the stronger hemolysis of human erythrocytes was observed with the CR-mGO2 (Supporting Information Figure S12c). Obviously, hydrophobic interaction plays a critical role in the interaction of the mGO with AQP1 because the amine-modified mGO could induce the formation of vacuoles, as well (Supporting Information Figure S16). In principle, such hydrophobic interaction between AQP1 and mGO could also happen between other membrane proteins and mGO. However, besides the formation of vacuoles, no other phenotype features were observed in the cell lines tested, which implies that other techniques may be necessary to explore that. Whether or not the conclusion is applicable to other types of membrane proteins remains to be discovered through detailed biological study, which is currently underway in our laboratory.

In theory, such types hydrophobic interactions could also occur between the membrane lipid and mGO.[55] Actually, it was reported that the tail end of a GO nanosheet is possibly trapped by the membranes due to strong van der Waals attractions from the membrane lipids and GO interactions, thus the permeability of the membrane could be affected.[22] To inspect whether the membrane permeability of the cells was also affected under this condition, the MCF-7 cells were dyed with Annexin V-FITC and propidium iodide (PI)

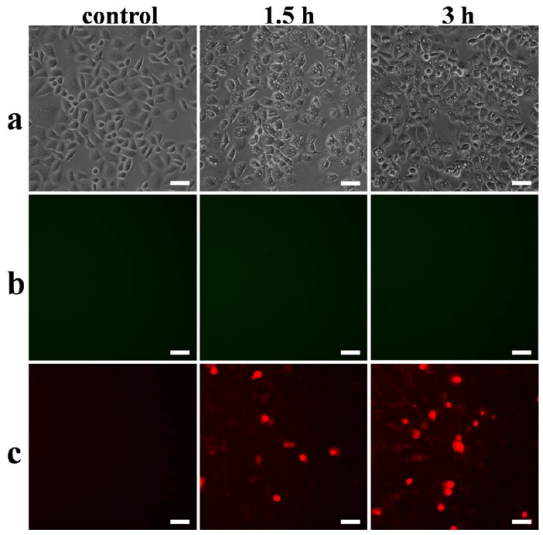

Figure 8. mGO treatment improves the cell permeability. (a) Microscopy images of the MCF-7 cells that were treated without and with mGO (100 μg mL^{-1}) for 1.5 and 3 h. (b) Fluorescence images of the cells stained with 2 μL of Annexin V-FITC for 10 min of incubation. (c) Cells were incubated with propidium iodide (10 μg mL^{-1}) for another 3 min. Scale bar: 50 μm.

after the pretreatment with the mGO.[56] Figure 8 displays the fluorescence images of the dyed cells with and without pretreatment of mGO. No fluorescence of Annexin V-FITC was observed in the control and the mGO-treated cells, meaning that no apoptosis occurred under the experimental conditions, which is in line with the proliferation assay result (Figure 3). In contrast, in the mGO-pretreated cells, the fluorescence of PI was observed, and the fluorescence intensity of PI increased with the incubation time, revealing that the permeability of the cell membrane was enhanced, which is in agreement with the penetration of LY observed in Figure 5. The penetration improvement to the cells was also observed in the uptake of rhodamine 123 (Supporting Information Figure S17). However, the permeability of the cell membrane was not markedly enhanced because a majority of GFP protein cannot penetrate the mGO-treated cells (Supporting Information Figure S18). On the other hand, it was known that the AQPs are imbedded tightly in the membrane,[49] thus the change in the membrane induced by mGO could possibly affect the conformation of AQPs, which may contribute partially to the enhanced water influx induced by the mGO. The membrane permeability change in the MCF-7 cells revealed that the interaction between mGO and the cell membrane did exist. The result was further supported by the fact that mGO enhanced cell permeability of the U87-MG cells in which expression of AQP1 is low (Supporting Information Figure S19).[51] Altogether, the accumulation of phase-lucent vacuoles is consistently observed in the tested cell lines that strongly express AQP1 (Supporting Information Figure S14), confirming that they are the consequences of the interaction of the mGO with AQP1. For those cells that weakly express AQP1, the mGO likely perturbs primarily the cell membrane. The findings that the mGO-treated cells (expressing AQP1) are vulnerable to vacuolization and have high cell permeability are potentially valuable in cancer therapy because AQPs are strongly expressed in tumor cells of different origins, particularly aggressive tumors.[57] Recently, it was demonstrated that the AQP expression is involved in more advanced clinical progression of breast cancer and might be a biomarker and potential therapeutic target for breast cancer.[44] In addition, the enhanced cell permeability by mGO suggests that the mGO could be used as an agonist of AQPs, which will be beneficial for drug transport across barrier membranes, such as the blood–brain barrier.[24]

CONCLUSION

In this work, the interaction of the mGO, used often in biomedical research, with cells at the molecular level was inspected through variety of techniques. Different from the cellular uptake that was generally believed, the mGO sheets were not taken by the cells when they were exposed to the cells for a short time. Instead, the mGO sheets interact with the membrane and membrane protein AQP1, eliciting a cellular response. Within a short exposure time, the cell permeability was enhanced, and vacuoles were formed in the cytosolic compartment. The former effect is primarily contributed by the distortion of the cell membrane as a theoretical prediction,[22] while the latter was the result of the interaction of mGO with AQP1. The fact that these unexpected phenomena were only observed in the cells that strongly express AQP1 further confirmed the interaction of AQP1 with mGO. The formation of vacuoles being associated with the activity of AQP1 suggests that mGO could be used to tune the water transport of cells without severe cytotoxicity.[17] Owing to the fact that AQPs are strongly expressed in many tumor cell lines of different origins, the findings are potentially valuable in cancer therapy and have begun to be explored;[24] it also will be beneficial for drug transport across barrier membranes for mGO which could enhance cell permeability.

MATERIALS AND METHODS

Cell Culture, TEM, and Microscopy Imaging and Cell Viability and Toxicity Assay. Human breast cancer MCF-7 cells were cultured in RPMI 1640 with 10% newborn calf serum and 1% antibiotics (penicillin and streptomycin) at 37 °C under 5% CO_2. Human glioma cells U87-MG and U251-MG were cultured in Dulbecco's modified Eagle medium (DMEM) supplemented with 10%

newborn calf serum and 1% antibiotics. Glioma cells were kind gifts from Prof. Weilin Jin (Shanghai Jiao Tong University). For microscopy imaging, the MCF-7 cells were seeded in a 24-well plate with the density of 5×10^4 cells per well 24 h prior to use. For aquaporins' inhibition assay, MCF-7 cells were preincubated with 200 μM $HgCl_2$ and dispersed in RPMI 1640 for 7 min before the mGO treatment. Autophagy inhibition was realized by preincubation with 10 mM of 3-MA. The images of cells were captured by a phase-contrast inverted microscope (Nikon ECLIPSE, TS100). The control cells and experimental groups were incubated with the tracer lucifer yellow (Sigma, 0.5 mg mL^{-1} in PBS) for 15 min and immediately captured by microscopy after removal of the LY. The procedures for TEM sample preparation and measurement were the same as those previously described.[17] Briefly, the MCF-7 cells treated with 200 μg mL^{-1} of mGO were washed with PBS three times carefully. After fixation, negative staining, and dehydration, the cells were put into resin to finally obtain a resin block. The resin block was sliced into ultrathin sections. These sections were transferred onto a copper grid for TEM measurement (FEI, USA, Tecnai G2 Spirit BioTWIN).

The viability and toxicity assay was performed according to the literature.[58] MCF-7 cells were seeded in 96-well plates with 4000 cells per well. The cells were incubated with 20, 50, 100, and 200 μg mL^{-1} of GO for 24 h. After being washed with PBS, fresh culture medium with 20 μL of MTT (5 mg mL^{-1}) was added in each well. Four hours later, the suspensions were replaced with 200 μL of dimethylsulfoxide to dissolve the insoluble formazan, and the cell viability of each group was determined by measuring their absorbance at 490 nm using a thermo multiskan MK3 ELISA plate reader.

Cell Cycle Analysis. The MCF-7 cells that were pretreated with mGO for 3 h were fixed for 24 h in 70% ethanol at −20 °C. The cells were washed with PBS and stained with 50 μg mL^{-1} of propidium iodide containing RNase (100 μg mL^{-1}), incubated at 37 °C for 30 min, and then measured by FACS Calibur (BD Biosciences, Mountain View, CA). The procedure was the same with the control group and the experimental group after being recultured in complete culture medium. The G1, S, and G2/M populations were quantified by Flowjo 7.6.1 software.[59] The status of the cells was imaged by microscopy before harvest.

Cell Staining and Imaging. The MCF-7 cells were seeded on the collagen-coated Φ14 mm coverslips at a density of 2×10^5 cells per well in 24-well plates. The cells were transiently transfected with PSICOR-GFP or GFP-LC3 plasmid. The transfection complexes were prepared by mixing 0.8 μg of plasmid with 2 μL of Hieff Trans transfection reagent (YEASEN, USA) in culture medium. To remove the transfection complexes, the medium was replaced with complete culture medium 5 h later. The cells 24 h post-transfection were treated with mGO (20 μg mL^{-1}) for an additional 3 h. The MCF-7 cells were stained with 50 nM of lysotracker red (Beyotime, China) for 2 h to locate the lysosomes. CLSM images were captured under 488 nm excitation. Gauging the locations of LC3 puncta and lysosomes through a confocal laser scanning microscope (A1R, Nikon, Japan) was under 405 and 561 nm excitation, respectively.

Hemolysis of Red Blood Cells. Fresh ethylenediaminetetraacetic acid-stabilized human whole blood samples were collected from a healthy volunteer. Typically, 1 mL of whole blood was added to 2 mL of PBS and centrifuged at 500*g* for 10 min to isolate red blood cells (RBCs) from serum. This purification step was repeated five times, and then RBCs were dispersed in PBS. To test the hemolytic activity, 500 μL of RBC suspension (around 4×10^8 cells mL^{-1}) was cultured in mGO or CR-mGO suspension solutions in PBS at the concentrations from 20 to 200 μg mL^{-1}. For $HgCl_2$ inhibition, RBCs were preincubated with $HgCl_2$ for 10 min and then replaced with the medium containing mGO. Samples of RBCs suspended in deionized water and PBS were used as the positive control and negative control, respectively. All the samples were placed on a rocking shaker in an incubator at 37 °C for 1.5 h. After incubation, the samples were centrifuged at 10 016*g* for 5 min. The hemoglobin absorbance in the supernatant was measured at 570 nm, with 630 nm as a reference, using a thermo multiscan MK3 ELISA plate reader. Each experiment was repeated three times. Percentage of hemolysis was calculated according to the literature.[50]

mRNA Isolation and PCR. Total RNA was extracted from the U87 and U251 cells using total RNA extraction reagent (Vazyme Biotech, China). RNA quality was determined by electrophoresis (1.5% agarose gels). The cDNA was synthesized and amplified using the HiScript II One Step RT-PCR kit (Vazyme Biotech, China) according to the manufacturer's instruction. Oligonucleotide primers (Sangon Biotech, China) were designed for AQP1 (forward GGC CAC GAC CCT CTT TGT CTT CAT, reverse TCC CAC AGC CAG TGT AGT CAA TAG) and GAPDH (forward CTT TGG TAT CGT GGA AGGA, reverse CAC CCT GTT GCT GTA GCC). Then, 0.1 μg of mRNA was included in the PCR reaction. PCR conditions were as follows: denaturation at 94 °C for 5 min followed by 35 cycles at 94 °C for 30 s, 56 °C for 30 s, 72 °C for 1 min, with a final extension at 72 °C for 10 min. Amplified products were examined by electrophoresis (1.5% agarose gel) .

Western Blot Analysis. Confluent dishes of U87-MG, U-251-MG, MCF-7, and A549 cells were lysed and harvested in RIPA buffer (50 mM of Tris-HCl, pH 7.5, 150 mM of NaCl, 1% of Triton X-100, 1% of sodium dodecyl sulfate, SDS) supplemented with protease inhibitor (Roche, Swiss). Protein quantification was performed using a BCA assay kit (Beyotime, China). Samples were loaded onto a 10% SDS-PAGE (polyacrylamide gel electrophoresis) gel. The gel was transferred at 200 mA for 2 h at room temperature onto polyvinylidine difluoride paper (Beyotime, China). Membranes were blocked in blocking buffer (5% dried milk in Tris-buffered saline plus 0.05% Tween 20), incubated overnight with the primary monoclonal antibody AQP1 (Santa Cruz, CA) at 1:1000 at 4 °C, washed 5 × 5 min, incubated in horseradish peroxidase-conjugated secondary antibodies (Beyotime, China) at 1:1000 for 1 h followed by another round of washing (5 × 10 min), and reacted with chemiluminescence detection reagent (Beyotime, China) for an additional 3 min. The protein was visualized by exposure to a luminescence detection system (Tanon, China).

Conflict of Interest: The authors declare no competing financial interest.

Acknowledgment. This research was carried out with financial support from the national "973 Program" of China (Nos. 2014CB260411, 2015CB931801), National Science foundation of China (No. 11374205), the State Key Laboratory of Bioreactor Engineering (No. 2060204), 111 Project (No. B07023), the Shanghai Committee of Science and Technology (Nos. 11DZ2260600 and 12 nm0503500), and national "863" Program of China (No. 2012AA022603) for financial support of this work. J. Zhang and S. Guo designed the project. C. Wu, C. Wang, and C. Luo carried out the molecular level experiments. C. Wu prepared and characterized the mGO. J. Zheng contributed to the nerve cell related experiments. C. Luo and Y. Li carried out Western and RT-PCR experiments. J. Zhang, S. Guo, and C. Wu wrote the manuscript.

Supporting Information Available: Additional details as described in the text. The Supporting Information is available free of charge on the ACS Publications website at DOI: 10.1021/acsnano.5b01685.

REFERENCES AND NOTES

1. Bao, H.; Pan, Y.; Ping, Y.; Sahoo, N. G.; Wu, T.; Li, L.; Li, J.; Gan, L. H. Chitosan-Functionalized Graphene Oxide as a Nanocarrier for Drug and Gene Delivery. *Small* **2011**, *7*, 1569–1578.
2. Sun, X.; Liu, Z.; Welsher, K.; Robinson, J. T.; Goodwin, A.; Zaric, S.; Dai, H. Nano-Graphene Oxide for Cellular Imaging and Drug Delivery. *Nano Res.* **2008**, *1*, 203–212.
3. Zhang, L.; Xia, J.; Zhao, Q.; Liu, L.; Zhang, Z. Functional Graphene Oxide as a Nanocarrier for Controlled Loading and Targeted Delivery of Mixed Anticancer Drugs. *Small* **2010**, *6*, 537–544.
4. Zhang, L.; Lu, Z.; Zhao, Q.; Huang, J.; Shen, H.; Zhang, Z. Enhanced Chemotherapy Efficacy by Sequential Delivery of Sirna and Anticancer Drugs Using Pei-Grafted Graphene Oxide. *Small* **2011**, *7*, 460–464.

5. Kim, H.; Namgung, R.; Singha, K.; Oh, I. K.; Kim, W. J. Graphene Oxide-Polyethylenimine Nanoconstruct as a Gene Delivery Vector and Bioimaging Tool. *Bioconjugate Chem.* **2011**, *22*, 2558–2567.
6. Peng, C.; Hu, W.; Zhou, Y.; Fan, C.; Huang, Q. Intracellular Imaging with a Graphene-Based Fluorescent Probe. *Small* **2010**, *6*, 1686–1692.
7. Shi, X.; Gong, H.; Li, Y.; Wang, C.; Cheng, L.; Liu, Z. Graphene-Based Magnetic Plasmonic Nanocomposite for Dual Bioimaging and Photothermal Therapy. *Biomaterials* **2013**, *34*, 4786–4793.
8. Guo, C.; Book-Newell, B.; Irudayaraj, J. Protein-Directed Reduction of Graphene Oxide and Intracellular Imaging. *Chem. Commun. (Cambridge, U. K.)* **2011**, *47*, 12658–12660.
9. Shen, H.; Liu, M.; He, H.; Zhang, L.; Huang, J.; Chong, Y.; Dai, J.; Zhang, Z. Pegylated Graphene Oxide-Mediated Protein Delivery for Cell Function Regulation. *ACS Appl. Mater. Interfaces* **2012**, *4*, 6317–6323.
10. Tian, B.; Wang, C.; Zhang, S.; Feng, L.; Liu, Z. Photothermally Enhanced Photodynamic Therapy Delivered by Nano-Graphene Oxide. *ACS Nano* **2011**, *5*, 7000–7009.
11. Yang, K.; Zhang, S.; Zhang, G.; Sun, X.; Lee, S. T.; Liu, Z. Graphene in Mice: Ultrahigh *in Vivo* Tumor Uptake and Efficient Photothermal Therapy. *Nano Lett.* **2010**, *10*, 3318–3323.
12. Ren, H.; Wang, C.; Zhang, J.; Zhou, X.; Xu, D.; Zheng, J.; Guo, S. DNA Cleavage System of Nanosized Graphene Oxide Sheets and Copper Ions. *ACS Nano* **2010**, *4*, 7169–7174.
13. Zhou, X.; Zhang, Y.; Wang, C.; Wu, X.; Yang, Y.; Zheng, B.; Wu, H.; Guo, S.; Zhang, J. Photo-Fenton Reaction of Graphene Oxide: A New Strategy to Prepare Graphene Quantum Dots for DNA Cleavage. *ACS Nano* **2012**, *6*, 6592–6599.
14. Jia, X.; Hofmann, M.; Meunier, V.; Sumpter, B. G.; Campos-Delgado, J.; Romo-Herrera, J. M.; Son, H.; Hsieh, Y. P.; Reina, A.; Kong, J.; et al. Controlled Formation of Sharp Zigzag and Armchair Edges in Graphitic Nanoribbons. *Science* **2009**, *323*, 1701–1705.
15. Qu, G.; Liu, S.; Zhang, S.; Wang, L.; Wang, X.; Sun, B.; Yin, N.; Gao, X.; Xia, T.; Chen, J. J.; et al. Graphene Oxide Induces Toll-Like Receptor 4 (Tlr4)-Dependent Necrosis in Macrophages. *ACS Nano* **2013**, *7*, 5732–5745.
16. Mu, Q.; Su, G.; Li, L.; Gilbertson, B. O.; Yu, L. H.; Zhang, Q.; Sun, Y. P.; Yan, B. Size-Dependent Cell Uptake of Protein-Coated Graphene Oxide Nanosheets. *ACS Appl. Mater. Interfaces* **2012**, *4*, 2259–2266.
17. Wu, C.; Wang, C.; Han, T.; Zhou, X.; Guo, S.; Zhang, J. Insight into the Cellular Internalization and Cytotoxicity of Graphene Quantum Dots. *Adv. Healthcare Mater.* **2013**, *2*, 1613–1619.
18. Liu, Y.; Luo, Y.; Wu, J.; Wang, Y.; Yang, X.; Yang, R.; Wang, B.; Yang, J.; Zhang, N. Graphene Oxide Can Induce *in Vitro* and *in Vivo* Mutagenesis. *Sci. Rep.* **2013**, *3*, 3469–3476.
19. Yue, H.; Wei, W.; Yue, Z.; Wang, B.; Luo, N.; Gao, Y.; Ma, D.; Ma, G.; Su, Z. The Role of the Lateral Dimension of Graphene Oxide in the Regulation of Cellular Responses. *Biomaterials* **2012**, *33*, 4013–4021.
20. Wei, Y.; Wang, B.; Wu, J.; Yang, R.; Dunn, M. L. Bending Rigidity and Gaussian Bending Stiffness of Single-Layered Graphene. *Nano Lett.* **2013**, *13*, 26–30.
21. Li, Y.; Yuan, H.; von dem Bussche, A.; Creighton, M.; Hurt, R. H.; Kane, A. B.; Gao, H. Graphene Microsheets Enter Cells through Spontaneous Membrane Penetration at Edge Asperities and Corner Sites. *Proc. Natl. Acad. Sci. U. S. A.* **2013**, *110*, 12295–12300.
22. Tu, Y.; Lv, M.; Xiu, P.; Huynh, T.; Zhang, M.; Castelli, M.; Liu, Z.; Huang, Q.; Fan, C.; Fang, H.; et al. Destructive Extraction of Phospholipids from Escherichia Coli Membranes by Graphene Nanosheets. *Nat. Nanotechnol.* **2013**, *8*, 594–601.
23. Chen, J.; Peng, H.; Wang, X.; Shao, F.; Yuan, Z.; Han, H. Graphene Oxide Exhibits Broad-Spectrum Antimicrobial Activity against Bacterial Phytopathogens and Fungal Conidia by Intertwining and Membrane Perturbation. *Nanoscale* **2014**, *6*, 1879–1889.
24. Verkman, A. S.; Anderson, M. O.; Papadopoulos, M. C. Aquaporins: Important but Elusive Drug Targets. *Nat. Rev. Drug Discovery* **2014**, *13*, 259–277.
25. Zhang, J.; Yang, H.; Shen, G.; Cheng, P.; Zhang, J.; Guo, S. Reduction of Graphene Oxide Via L-Ascorbic Acid. *Chem. Commun. (Cambridge, U. K.)* **2010**, *46*, 1112–1114.
26. Zhou, X.; Zhang, J.; Wu, H.; Yang, H.; Zhang, J.; Guo, S. Reducing Graphene Oxide Via Hydroxylamine: A Simple and Efficient Route to Graphene. *J. Phys. Chem. C* **2011**, *115*, 11957–11961.
27. Liu, Q.; Wei, L.; Wang, J.; Peng, F.; Luo, D.; Cui, R.; Niu, Y.; Qin, X.; Liu, Y.; Sun, H.; et al. Cell Imaging by Graphene Oxide Based on Surface Enhanced Raman Scattering. *Nanoscale* **2012**, *4*, 7084–7089.
28. Ashford, T. P.; Porter, K. R. Cytoplasmic Components in Hepatic Cell Lysosomes. *J. Cell Biol.* **1962**, *12*, 198–202.
29. Klionsky, D. J.; Abeliovich, H.; Agostinis, P.; Agrawal, D. K.; Aliev, G.; Askew, D. S.; Baba, M.; Baehrecke, E. H.; Bahr, B. A.; Ballabio, A.; et al. Guidelines for the Use and Interpretation of Assays for Monitoring Autophagy in Higher Eukaryotes. *Autophagy* **2008**, *4*, 151–175.
30. Kroemer, G.; Galluzzi, L.; Vandenabeele, P.; Abrams, J.; Alnemri, E. S.; Baehrecke, E. H.; Blagosklonny, M. V.; El-Deiry, W. S.; Golstein, P.; Green, D. R.; et al. Classification of Cell Death: Recommendations of the Nomenclature Committee on Cell Death 2009. *Cell Death Differ.* **2009**, *16*, 3–11.
31. Seglen, P. O.; Gordon, P. B. 3-Methyladenine: Specific Inhibitor of Autophagic/Lysosomal Protein Degradation in Isolated Rat Hepatocytes. *Proc. Natl. Acad. Sci. U. S. A.* **1982**, *79*, 1889–1892.
32. Patterson, G. H.; Lippincott-Schwartz, J. Selective Photolabeling of Proteins Using Photoactivatable Gfp. *Methods* **2004**, *32*, 445–450.
33. Li, Y.; Wu, Q.; Zhao, Y.; Bai, Y.; Chen, P.; Xia, T.; Wang, D. Response of Micrornas to *in Vitro* Treatment with Graphene Oxide. *ACS Nano* **2014**, *8*, 2100–2110.
34. Huang, J.; Zong, C.; Shen, H.; Liu, M.; Chen, B.; Ren, B.; Zhang, Z. Mechanism of Cellular Uptake of Graphene Oxide Studied by Surface-Enhanced Raman Spectroscopy. *Small* **2012**, *8*, 2577–2584.
35. Chang, Y.; Yang, S. T.; Liu, J. H.; Dong, E.; Wang, Y.; Cao, A.; Liu, Y.; Wang, H.; et al. Toxicity Evaluation of Graphene Oxide on A549 Cells. *Toxicol. Lett.* **2011**, *200*, 201–210.
36. Kabeya, Y.; Mizushima, N.; Ueno, T.; Yamamoto, A.; Kirisako, T.; Noda, T.; Kominami, E.; Ohsumi, Y.; Yoshimori, T. Lc3, a Mammalian Homologue of Yeast Apg8p, Is Localized in Autophagosome Membranes after Processing. *EMBO J.* **2000**, *19*, 5720–5728.
37. Goranov, A. I.; Cook, M.; Ricicova, M.; Ben-Ari, G.; Gonzalez, C.; Hansen, C.; Tyers, M.; Amon, A. The Rate of Cell Growth Is Governed by Cell Cycle Stage. *Genes Dev.* **2009**, *23*, 1408–1422.
38. Sakaue-Sawano, A.; Kurokawa, H.; Morimura, T.; Hanyu, A.; Hama, H.; Osawa, H.; Kashiwagi, S.; Fukami, K.; Miyata, T.; Miyoshi, H.; et al. Visualizing Spatiotemporal Dynamics of Multicellular Cell-Cycle Progression. *Cell* **2008**, *132*, 487–498.
39. Elledge, S. J. Cell Cycle Checkpoints: Preventing an Identity Crisis. *Science* **1996**, *274*, 1664–1672.
40. Reuss, L. Water Transport across Cell Membranes. *eLS* **2012**, DOI: 10.1002/9780470015902.a0020621.pub2.
41. Bar-Sagi, D.; Feramisco, J. R. Induction of Membrane Ruffling and Fluid-Phase Pinocytosis in Quiescent Fibroblasts by Ras Proteins. *Science* **1986**, *233*, 1061–1068.
42. Swanson, J. A.; Watts, C. Macropinocytosis. *Trends Cell Biol.* **1995**, *5*, 424–428.
43. Otterbach, F.; Callies, R.; Adamzik, M.; Kimmig, R.; Siffert, W.; Schmid, K. W.; Bankfalvi, A. Aquaporin 1 (Aqp1) Expression Is a Novel Characteristic Feature of a Particularly Aggressive Subgroup of Basal-Like Breast Carcinomas. *Breast Cancer Res. Treat.* **2010**, *120*, 67–76.
44. Shi, Z.; Zhang, T.; Luo, L.; Zhao, H.; Cheng, J.; Xiang, J.; Zhao, C. Aquaporins in Human Breast Cancer: Identification and Involvement in Carcinogenesis of Breast Cancer. *J. Surg. Oncol.* **2012**, *106*, 267–272.

45. Preston, G. M.; Jung, J. S.; Guggino, W. B.; Agre, P. The Mercury-Sensitive Residue at Cysteine 189 in the Chip28 Water Channel. *J. Biol. Chem.* **1993**, *268*, 17–20.
46. Niemietz, C. M.; Tyerman, S. D. New Potent Inhibitors of Aquaporins: Silver and Gold Compounds Inhibit Aquaporins of Plant and Human Origin. *FEBS Lett.* **2002**, *531*, 443–447.
47. Ma, B.; Xiang, Y.; Mu, S. M.; Li, T.; Yu, H. M.; Li, X. J. Effects of Acetazolamide and Anordiol on Osmotic Water Permeability in Aqp1-Crna Injected Xenopus Oocyte. *Acta Pharmacol. Sin.* **2004**, *25*, 90–97.
48. Murata, K.; Mitsuoka, K.; Hirai, T.; Walz, T.; Agre, P.; Heymann, J. B.; Engel, A.; Fujiyoshi, Y. Structural Determinants of Water Permeation through Aquaporin-1. *Nature* **2000**, *407*, 599–605.
49. Denker, B. M.; Smith, B. L.; Kuhajda, F. P.; Agre, P. Identification, Purification, and Partial Characterization of a Novel Mr 28,000 Integral Membrane Protein from Erythrocytes and Renal Tubules. *J. Biol. Chem.* **1988**, *263*, 15634–15642.
50. Liao, K. H.; Lin, Y. S.; Macosko, C. W.; Haynes, C. L. Cytotoxicity of Graphene Oxide and Graphene in Human Erythrocytes and Skin Fibroblasts. *ACS Appl. Mater. Interfaces* **2011**, *3*, 2607–2615.
51. McCoy, E.; Sontheimer, H. Expression and Function of Water Channels (Aquaporins) in Migrating Malignant Astrocytes. *Glia* **2007**, *55*, 1034–1043.
52. Gravelle, S.; Joly, L.; Detcheverry, F.; Ybert, C.; Cottin-Bizonne, C.; Bocquet, L. Optimizing Water Permeability through the Hourglass Shape of Aquaporins. *Proc. Natl. Acad. Sci. U. S. A.* **2013**, *110*, 16367–16372.
53. Wang, S.; Zhang, Y.; Abidi, N.; Cabrales, L. Wettability and Surface Free Energy of Graphene Films. *Langmuir* **2009**, *25*, 11078–11081.
54. Zhang, Y.; Zhang, J.; Huang, X.; Zhou, X.; Wu, H.; Guo, S. Assembly of Graphene Oxide-Enzyme Conjugates through Hydrophobic Interaction. *Small* **2012**, *8*, 154–159.
55. Titov, A. V.; Kral, P.; Pearson, R. Sandwiched Graphene--Membrane Superstructures. *ACS Nano* **2010**, *4*, 229–234.
56. Qu, G.; Wang, X.; Wang, Z.; Liu, S.; Jiang, G. Cytotoxicity of Quantum Dots and Graphene Oxide to Erythroid Cells and Macrophages. *Nanoscale Res. Lett.* **2013**, *8*, 198.
57. Verkman, A. S.; Hara-Chikuma, M.; Papadopoulos, M. C. Aquaporins--New Players in Cancer Biology. *J. Mol. Med. (Heidelberg, Ger.)* **2008**, *86*, 523–529.
58. Mosmann, T. Rapid Colorimetric Assay for Cellular Growth and Survival: Application to Proliferation and Cytotoxicity Assays. *J. Immunol. Methods* **1983**, *65*, 55–63.
59. Austin, L. A.; Kang, B.; Yen, C. W.; El-Sayed, M. A. Nuclear Targeted Silver Nanospheres Perturb the Cancer Cell Cycle Differently Than Those of Nanogold. *Bioconjugate Chem.* **2011**, *22*, 2324–2331.